Research Article Vol. 2, No. 7 / 15 July 2019 / OSA Continuum 2137

Electromagnetically induced transparency in terahertz complementary spiral-shape metamaterials

SHAOJUN CHENG, ZEFENG XU, DONGYUAN YAO, XIAO ZHANG, ZHI ZHANG, AND YU-SHENG LIN*

State Key Laboratory of Optoelectronic Materials and Technologies, School of Electronics and Information Technology, Sun Yat-Sen University, Guangzhou 510275, China
linyoush@mail.sysu.edu.cn

Abstract: We propose and demonstrate two designs of complementary spiral-shape metamaterials (CSSM) with square and hexagonal meta-atom arrangements in the terahertz (THz) frequency range. For convenience, they are denoted as CSSM-S and CSSM-H for CSSM with square and hexagonal meta-atom arrangements, respectively. The electromagnetic responses are investigated for CSSM with different spiral angle (θ). CSSM-S exhibits dual-, triple-, and quad-resonance for $\theta = 360°$, $\theta = 540°$ and $\theta = 720°$, respectively in transverse electric (TE) mode and exhibits single-, dual-, and triple-resonance for $\theta = 360°$, $\theta = 540°$ and $\theta = 720°$, respectively in transverse magnetic (TM) mode. By applying a direct-current (dc) bias voltage on CSSM-S, it shows the actively tunable resonance with a tuning range of 0.12 THz and switching polarization characteristics. Furthermore, to facilitate the flexibility and applicability of CSSM, the unit cell of CSSM with different θ is superimposed to form CSSM-H. CSSM-H possesses the combination of electromagnetic behaviors generated by each unit cell of CSSM with different θ. This study provides a design of complementary THz metamaterials to have electromagnetically induced transparency (EIT) analog characteristics, which shows single-digital and multi-digital signals for the programmable metamaterial application. It paves a way to the possibility of THz metamaterials with great tunability and good polarization-dependence.

1. Introduction

Terahertz (THz) wave is the transition spectrum from microwave to infrared (IR) wavelength which occupies the spectrum in the frequency range of 0.1 THz to 10 THz [1–3]. Among the entire electromagnetic spectrum, THz optics in spectroscopy and imaging systems is imperative to THz wave applications, such as quality control, security check, physics study, and molecule identification [4–6]. Moreover, the integration of THz optics constituted by miniaturized optical components is expected to express higher signal transportation [7]. It allows more compact systems and enables the integration with other systems for increasing flexibility and applicability. For instance, THz device can be compacted into semiconductor integrated circuits and integrated photonic circuits [8,9]. Such miniaturized THz optical components are required new approaches and techniques for the realization of active manipulation to possess multi-functionalities.

Over the past two decades, the artificially electromagnetic material, termed metamaterial, has attracted a tremendous amount of attention for researchers owing to their exotic and extraordinary optical properties to manipulate the amplitude, direction, polarization, wavelength, and phase of electromagnetic waves [10–14]. By properly tailoring the geometrical dimension of metamaterial, it can be realized electro-optic devices spanning the frequency range from microwave, THz, IR, visible to ultraviolet caused from the transformation optics theory [15]. Therefore, many literatures have been reported unique electromagetic metamaterials which have largely improved many classic devices, such as switch, resonator, waveguide, filter and so on [16–23]. The

#358271 https://doi.org/10.1364/OSAC.2.002137
Journal © 2019 Received 1 Apr 2019; revised 21 May 2019; accepted 27 May 2019; published 26 Jun 2019

OSA CONTINUUM

unprecedented advantages of metamaterial come from its extreme scalability and ultrathin feature. Metamaterial has led to the demonstration of even exotic THz properties such as artificial magnetism, negative refractive index, wavelength perfect absorption, chirality, and electromagnetically induced transparency (EIT) [24–29]. Recently, the EIT analog using planar metamaterials have been demonstrated to enable the realization of slow light effect and high nonlinearity in THz frequency range, which are reported and performed through near-field coupling between the resonators at bright and dark modes by implanting extra materials into the unit cell of metamaterial [30,31]. The controllable methods are through dynamic modulation of resonator at dark mode [32] or the intercoupling distance [33], including optical pumping of photoconductive materials [34], or thermally controlled superconducting materials as the part of coupled resonator system [35]. Such tunability in coupled resonator system adds a new dimension to the design and functionality of metamaterial and possible applications [36].

In this study, we propose a design to control the EIT analog without implanted any extra material into the metamaterial structures. We design and utilize two types of THz complementary spiral-shape metamaterial (CSSM) with square and hexagonal meta-atom arrangements, which are denoted as CSSM-S and CSSM-H, respectively. The proposed devices possess EIT analog characteristics by controlling bright and dark modes within resonators. CSSM-S with different spiral angle (θ) exhibits dual-, triple-, and quad-resonance at transverse electric (TE) mode, while that shows single-, dual-, and triple-resonance at transverse magnetic (TM) mode, respectively. Furthermore, CSSM-H indicates the characteristics of tunable and switchable single-band and dual-band EIT analog. These electromagnetic characteristics provide the possibilities for the realization of programmable metamaterial in THz wave applications.

2. Designs and methods

The schematic drawing of CSSM-S is shown in Fig. 1(a). The unit cell and corresponding denotations of CSSM-S are indicated in Fig. 1(b). They are spiral angle (θ) and spiral width (w). Here, the spiral widths are 6 μm and the periods of devices are kept as constant as 100×100 μm^2 and 160×160 μm^2 for CSSM-S and CSSM-H, respectively. The proposed CSSM device was fabricated using maskless photolithography and lift-off techniques. First, the lift-off resistance was spin coated, which was polymethylmethacrylate (PMMA) spun on the device and baked at 180 °C for 2 min. Second, the metamaterial pattern was defined on the resist layer using a maskless photography technique. Third, the 10/200 nm thick Cr/Au layer was deposited on an

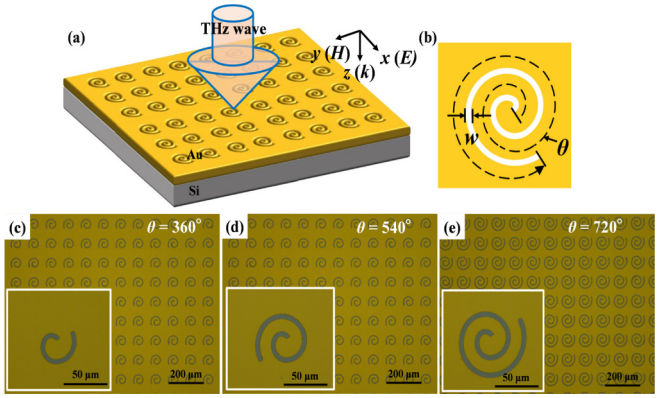

Fig. 1. Schematic drawing of CSSM-S. (b) The corresponding denotations of CSSM-S, where w is spiral width and θ is spiral angle. (c-e) are optical microscopy images of CSSM-S with $\theta = 360°$, $\theta = 540°$, and $\theta = 720°$, respectively.

OSA CONTINUUM

unintentional doping Si substrate using a sputtering system. After development of the resist in 3:1 isopropyl alcohol (IPA)/deionized water (DI) solution for 5 min, the CSSM pattern was performed by removing the resist. Figure 1(c-e) are optical microscopy images of spiral-shape array of CSSM-S with $\theta = 360°$, $\theta = 540°$, and $\theta = 720°$, respectively. The corresponding unit cells are shown in the inserted images of Fig. 1(c-e), respectively. The patterns are easily fabricated, high portability, applicability, and cost-effectiveness. The electromagnetic characteristics of CSSM-S and CSSM-H are performed by using Lumerical Solution's finite difference time-domain (FDTD) based simulations to study the optical properties of devices. The propagation direction of incident THz wave is perpendicular to the *x*-*y* plane in the numerical simulations. Periodic boundary conditions are also adopted in the *x* and *y* directions and perfectly matched layer (PML) boundaries conditions are assumed in the z direction. The mesh precision is 0.5 nm with the minimum clearance size of 0.1 μm. The transmission THz wave is calculated by setting monitor on the bottom side of device.

3. Results and discussions

Fig. 2 shows the transmission spectra of CSSM-S with different θ at TE and TM modes. In Fig. 2(a), there is no any resonance in the frequency range of 0.1-0.5 THz at TM mode. It can be seen there is a sharp transmission peak at 0.26 THz within the broad frequency range of 0.1-0.5 THz for CSSM-S with $\theta = 360°$. This is a signature of the strong plasmonic hybridization in the resonator system. It is the resonance of bright mode in EIT analog. It can be explained by the strong E-field energy focused on the spiral-shape of CSSM-S as shown in Fig. 3(a). The induced transmission intensity is switched from 0.11 to 0.65 by rotating incident polarization angle from TM mode to TE mode. Simultaneously, there is a dark mode at 0.27 THz. The transmission intensity could be switched from 0 (TM mode) to 0.11 (TE mode). Figure 2(b) shows the transmission spectra of CSSM-S with $\theta = 540°$. The transmission intensity of 0.28 at TM mode can be switched to 0.65 at TE mode to form the bright mode in EIT analog. The resonance is at 0.30 THz. While it can be also switched to the dark mode at 0.33 THz. For the case of CSSM-S with $\theta = 720°$ as shown in Fig. 2(c), there are bright modes at 0.17 THz (TE mode) and 0.45 THz (TM mode). While there are dark modes at 0.18 THz (TE mode) and 0.44 THz (TE mode). That can be switched between bright mode and dark mode by changing incident polarization light. To better understand the interactions of THz wave to the proposed CSSM-S, the electromagnetic field monitors are simulated and set into CSSM-S. The corresponding electric (E) field and magnetic (H) field distributions are represented in Fig. 3(a-f). The resonant frequency of the circuit model of CSSM-S can be expressed by [37]

$$f_{LC} = \frac{1}{2\pi P\sqrt{\varepsilon_c}}\sqrt{\frac{w}{l}} \tag{1}$$

where c_0 is the velocity of light in vacuum, ε_c is the relative permittivity of materials in the spiral shape (i.e. air in this study), P is the spiral period, w is the spiral width, and l is the spiral length. This complementary spiral-shape resonator is designed by the E-field energy strongly coupling into complementary spiral-shape microstructures, while the inductive element (the frames or the loops) does not interact with E- and H-field energies. It can be clearly observed that E-field energies are focused along the spiral-shape of CSSM-S to generate different resonances.

To further enhance the flexibility of proposed CSSM, it is designed to be controlled by applying a direct-current (dc) bias voltage to heating up the temperature of surrounding ambient. CSSM-S with $\theta = 720°$ is chosen to be an example for the realization of tunable CSSM. The schematic drawing of proposed tunable CSSM-S is shown in Fig. 4(a). The experimental results are shown in Fig. 4(b). The electromagnetic responses of CSSM-S at TM and TE modes without applying a dc bias voltage are identical to the results of Fig. 2. By increasing the dc bias voltage from 0 V to 30 V, the resonance is red-shift from 0.46 THz to 0.34 THz with a tuning range of 0.12 THz.

OSA CONTINUUM

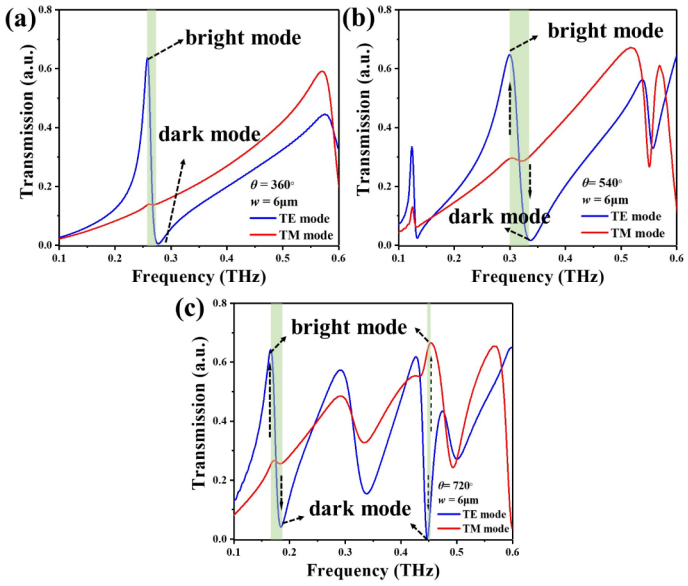

Fig. 2. Transmission spectra of CSSM-S with (a) $\theta = 360°$, (b) $\theta = 540°$, and (c) $\theta = 720°$ at TE and TM modes.

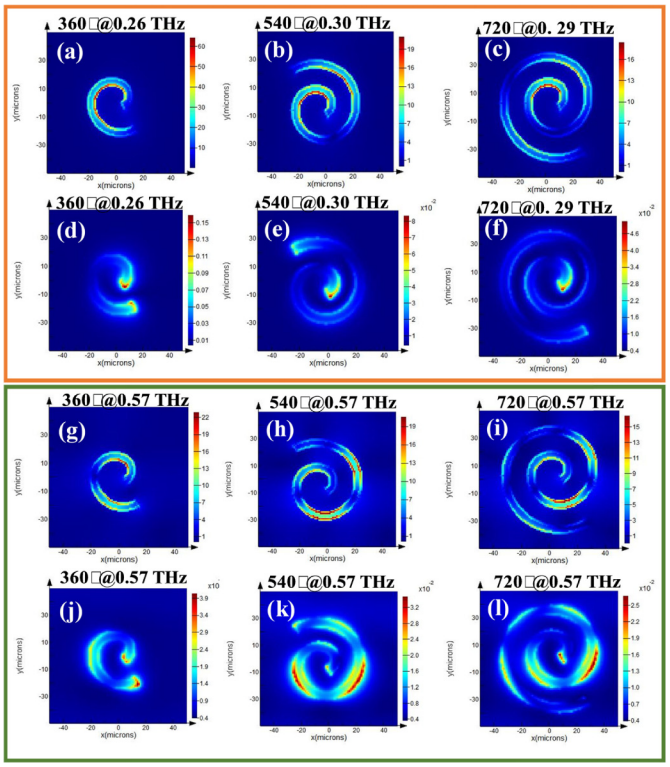

Fig. 3. (a-c) E-field and (d-f) H-field distributions of CSSM-S with different θ at TE mode, respectively. (g-i) E-field and (j-l) H-field distributions of CSSM-S with different θ at TM mode, respectively. The inserted denotations on top images are monitored frequencies for CSSM-S with different θ.

OSA CONTINUUM

The surrounding temperature is increased by applying a dc bias voltage on device, which can be expressed by [38]

$$T - T_0 = P \times R_s = \frac{V^2}{R_t} \times R_s = \frac{V^2}{R_0[1 + \alpha(T - T_0)]} \times R_s \tag{2}$$

where T_0 is the initial room-temperature, R_0 is the resistance at initial room-temperature, R_s is the thermal resistance from substrate to ambient environment, R_t is the resistance at heating temperature, α is the linear temperature coefficient of resistance. Owing to the variation of heating temperature can make the surrounding refraction index (n_s) changed, it can be obtained by [39]

$$\frac{1}{n_s}\frac{dn}{dT} = -\frac{(n_s^2 - 1)E_g}{(n_s^2)E_g^2 - (h\gamma)^2} - \frac{3\beta n_s^2 - 1}{2n_s^2} \tag{3}$$

where γ is the frequency of the illumination light, h is Planck's constant, β is the thermal expansion coefficient for material, and E_g is the bandgap energy of material. Furthermore, the ambient refraction index is a key role parameter to determine the Fano-resonance of CSSM referred to the equation of $n_s = \sqrt{\varepsilon_r \mu_r}$, where ε_r and μ_r are the equivalent permittivity and permeability of CSSM, respectively. Such designed tuning approach indicates the possibility of CSSM to be used for filter, polarizer, switch, and sensor with active tuning characteristic in THz frequency range.

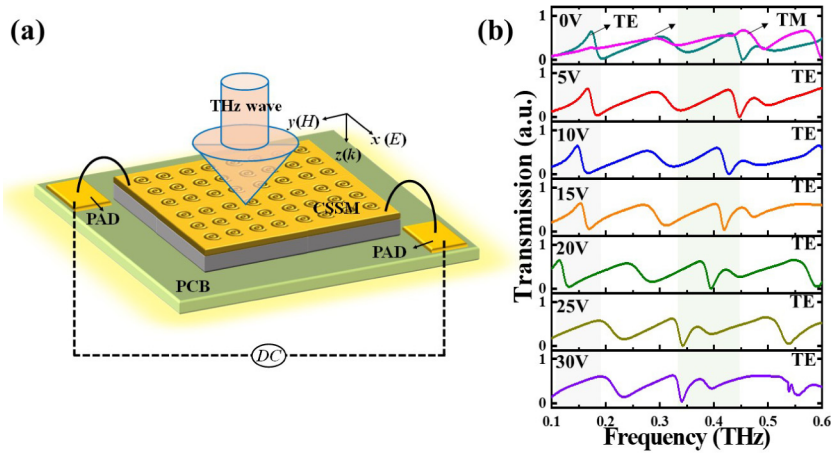

Fig. 4. (a) Schematic drawing of tunable CSSM-S applied a dc bias voltage. (b) Transmission spectra of CSSM-S applied a dc bias voltage from 0 V to 30 V at TE mode.

The electromagnetic responses of CSSM-H with $\theta = 360°$, $\theta = 540°$, $\theta = 720°$, and corresponding superimposed conditions are shown in Fig. 5. The simulated results of CSSM-H with $\theta = 360°$, $\theta = 540°$, and $\theta = 720°$ are shown in Fig. 5(a-c), respectively. In Fig. 5(a), CSSM-H with $\theta = 360°$ exhibits the bright-mode at 0.26 THz and dark-mode at 0.27 THz. The corresponding E-field and H-field distributions are shown in the inserted images of Fig. 5(a). In the design of CSSM-H with $\theta = 540°$, it exhibits the bright-mode at 0.30 THz and dark-mode at 0.33 THz as shown in Fig. 5(b). The corresponding E- and H-fields distributions are shown in the inserted images of Fig. 5(b). Moreover, CSSM-H with $\theta = 540°$ exhibits a polarization switch at 0.55 THz, which can be switched the transmission intensity from 0.05 at TM mode to 0.60 at TE mode. Figure 5(c) shows the results for the case of CSSM-H with $\theta = 720°$, which exhibits the bright-mode at 0.17 THz and dark-mode at 0.18 THz. The corresponding E-field and H-field distributions are shown in the inserted images of Fig. 5(c). For the cases of CSSM-H with superimposed different θ,

OSA CONTINUUM

the transmission spectra of CSSM-H with $\theta = 360°+540°$, $\theta = 360°+720°$, and $\theta = 540°+720°$ are shown in Fig. 5(d-f), respectively. Figure 5(d) shows the resonances of CSSM-H with $\theta = 360°+540°$ at 0.26 THz and 0.30 THz for bright-modes while at 0.27 THz and 0.32 THz for dark-modes, which are the superimposed results of Fig. 5(a) and Fig. 5(b). There is a little variation of 0.01 THz for dark-mode resonance caused from the continuous superimposed spectra. It is worth to noted that there are two polarization switching functions at 0.52 THz and 0.55 THz, respectively. In Fig. 5(e), there are two bright-modes at 0.17 THz and 0.26 THz and two dark-modes at 0.18 THz and 0.27 THz, respectively for the case of CSSM-H with $\theta = 360°+720°$. The corresponding E-field and H-field distributions are shown in the inserted images of Fig. 5(e). Figure 5(f) shows the transmission spectra of CSSM-H with $\theta = 540°+720°$. There are two bright-modes at 0.17 THz and 0.30 THz and two dark-modes at 0.18 THz and 0.33 THz, respectively. The corresponding E-field and H-field distributions are shown in the inserted images of Fig. 5(f). These results indicate that the EIT analog can be controlled by hexagonal meta-atom arrangement of CSSM to possess single-digital and multi-digital signals to increase the flexibility and capability for the realization of programmable metamaterials in THz frequency range.

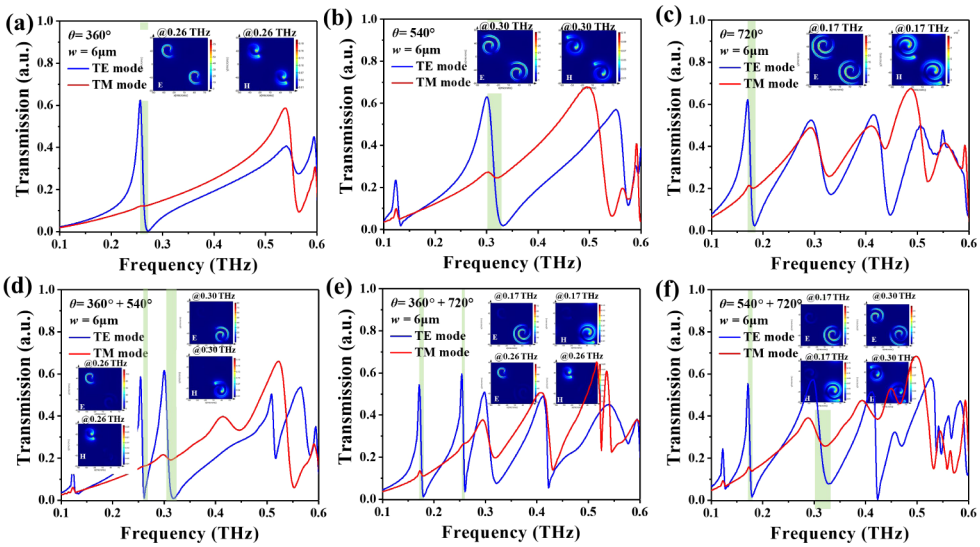

Fig. 5. Transmission spectra of CSSM-H with (a) $\theta = 360°$, (b) $\theta = 540°$, (c) $\theta = 720°$, (d) $\theta = 360°+540°$, (e) $\theta = 360°+720°$, and (f) $\theta = 540°+720°$ at TE and TM modes.

4. Conclusion

In conclusion, we present two CSSM designs with square and hexagonal meta-atom arrangements (CSSM-S and CSSM-H) which exhibit EIT analog characteristics. CSSM-S shows dual-, triple-, and quad-resonance for $\theta = 360°$, $\theta = 540°$, and $\theta = 720°$, respectively at TE mode and shows single-, dual-, and triple-resonance for $\theta = 360°$, $\theta = 540°$ and $\theta = 720°$, respectively at TM mode. These electromagnetic behaviors are polarization-dependence and EIT switch at different polarization state. CSSM-H indicates single-digital and multi-digital signals to lay the foundation for the realization of programmable metamaterials in THz frequency range. CSSM-S performs the tunable THz filter by applying a dc bias voltage on device. The tuning range is 0.12 THz compared to that without and with a dc bias voltage of 30 V. With the investigation of CSSM being fully understood, the design of CSSM exhibits the multi-functionalities of single-band and dual-band switch and polarization switch. It potentially provides a new direction for future

OSA CONTINUUM

THz device applications and a flexible platform for developing the next generation randomly accessible, digital and programmable metamaterials for precise tailoring of electromagnetic properties and multi-channel data processing at higher bit rates.

Funding

Research grants of the 100 Talents Program of Sun Yat-sen University (SYSU) (76120-18841202).

Acknowledgment

The authors acknowledge the State Key Laboratory of Optoelectronic Materials and Technologies of Sun Yat-Sen University for the uses of simulation codes and experimental equipment.

References

1. E. Manikandan, B. S. Sreeja, S. Radha, and R. N. Bathe, "Direct laser fabrication of five-band symmetric terahertz metamaterial with Fano resonance," Mater. Lett. **229**, 320–323 (2018).
2. C. R. Simovski, P. A. Belov, A. V. Atrashchenko, and Y. S. Kivshar, "Wire metamaterials: physics and applications," Adv. Mater. **24**(31), 4229–4248 (2012).
3. K. Shih, P. Pitchappa, L. Jin, C. H. Chen, R. Singh, and C. Lee, "Nanofluidic terahertz metasensor for sensing in aqueous environment," Appl. Phys. Lett. **113**(7), 071105 (2018).
4. M. Lee, H. E. Katz, C. Erben, D. M. Gill, P. Gopalan, J. D. Heber, and D. J. McGee, "Broadband modulation of light by using an electro-optic polymer," Science **298**(5597), 1401–1403 (2002).
5. R. Jiang, Z. R. Wu, Z. Y. Han, and H. S. Jung, "HfO2-based ferroelectric modulator of terahertz waves with graphene metamaterial," Chin. Phys. B **25**(10), 106803 (2016).
6. W. Xu, L. Xie, and Y. Ying, "Mechanisms and applications of terahertz metamaterial sensing: a review," Nanoscale **9**(37), 13864–13878 (2017).
7. H. T. Chen, W. J. Padilla, J. M. O. Aide, A. C. Gossard, A. J. Taylor, and R. D. Averitt, "Active terahertz metamaterial devices," Nature **444**(7119), 597–600 (2006).
8. D. R. Smith, J. B. Pendry, and M. C. K. Wiltshire, "Metamaterials and negative refractive index," Science **305**(5685), 788–792 (2004).
9. G. Liang and Q. J. Wang, "Integrated terahertz optoelectronics," Proc. SPIE **10030**, 100300T (2016).
10. S. Wang, L. Kang, and D. H. Werner, "Active Terahertz Chiral Metamaterials Based on Phase Transition of Vanadium Dioxide (VO2)," Sci. Rep. **8**(1), 189 (2018).
11. Y. Zhao, Y. Zhang, Q. Shi, S. Liang, W. Huang, W. Kou, and Z. Yang, "Dynamic Photoinduced Controlling of the Large Phase Shift of Terahertz Waves via Vanadium Dioxide Coupling Nanostructures," ACS Photonics **5**(8), 3040–3050 (2018).
12. Q. Y. Wen, H. W. Zhang, Q. H. Yang, Y. S. Xie, K. Chen, and Y. L. Liu, "Terahertz metamaterials with VO2 cut-wires for thermal tunability," Appl. Phys. Lett. **97**(2), 021111 (2010).
13. M. Unlu, M. R. Hashemi, C. W. Berry, S. Li, S. H. Yang, and M. Jarrahi, "Switchable scattering meta-surfaces for broadband terahertz modulation," Sci. Rep. **4**(1), 5708 (2015).
14. L. Huang, C. C. Chang, B. Zeng, J. Nogan, S. N. Luo, A. J. Taylor, A. K. Azad, and H. T. Chen, "Bilayer Metasurfaces for Dual- and Broadband Optical Antireflection," ACS Photonics **4**(9), 2111–2116 (2017).
15. Z. Xu, R. Xu, B. Zhang, Y. Tong, and Y. S. Lin, "Infrared metamaterial absorber by using chalcogenide glass material with a cyclic ring-disk structure," OSA Continuum **1**(2), 573–580 (2018).
16. S. Misra, L. Li, J. Jian, J. Huang, X. Wang, D. Zemlyanov, J. W. Jang, F. H. Ribeiro, and H. Wang, "Tailorable Au Nanoparticles Embedded in Epitaxial TiO2 Thin Films for Tunable Optical Properties," ACS Appl. Mater. Interfaces **10**(38), 32895–32902 (2018).
17. D. M. Wu, M. L. Solomon, G. V. Naik, A. Garcia-Etxarri, M. Lawrence, A. Salleo, and J. A. Dionne, "Chemically Responsive Elastomers Exhibiting Unity-Order Refractive Index Modulation," Adv. Mater. **30**(7), 1703912 (2018).
18. C. Yuan, X. Mu, C. K. Dunn, J. Haidar, T. Wang, and H. J. Qi, "Thermomechanically Triggered Two-Stage Pattern Switching of 2D Lattices for Adaptive Structures," Adv. Funct. Mater. **28**(18), 1705727 (2018).
19. M. Mittendorff, S. Li, and T. E. Murphy, "Graphene-Based Waveguide-Integrated Terahertz Modulator," ACS Photonics **4**(2), 316–321 (2017).
20. S. H. Lee, M. Choi, T. T. Kim, S. Lee, M. Liu, X. Yin, H. K. Choi, S. S. Lee, C. G. Choi, S. Y. Choi, X. Zhang, and B. Min, "Switching terahertz waves with gate-controlled active graphene metamaterials," Nat. Mater. **11**(11), 936–941 (2012).
21. B. Zhu, Y. J. Feng, J. M. Zhao, C. Huang, and T. A. Jiang, "Switchable metamaterial reflector/absorber for different polarized electromagnetic waves," Appl. Phys. Lett. **97**(5), 051906 (2010).
22. L. Q. Cong, P. Pitchappa, Y. Wu, L. Ke, C. Lee, N. Singh, H. Yang, and R. Singh, "Active Multifunctional Microelectromechanical System Metadevices: Applications in Polarization Control, Wavefront Deflection, and Holograms," Adv. Opt. Mater. **5**(2), 1600716 (2017).

OSA CONTINUUM

23. W. Xu, L. Xie, J. Zhu, X. Xu, Z. Ye, C. Wang, Y. Ma, and Y. Ying, "Gold Nanoparticle-Based Terahertz Metamaterial Sensors: Mechanisms and Applications," ACS Photonics **3**(12), 2308–2314 (2016).
24. Y. Bai, K. Chen, H. Liu, T. Bu, B. Cai, J. Xu, and Y. Zhu, "Optically controllable terahertz modulator based on electromagnetically-induced-transparency-like effect," Opt. Commun. **353**, 83–89 (2015).
25. Y. S. Lin, C. Y. Huang, and C. Lee, "Reconfiguration of Resonance Characteristics for Terahertz U-Shape Metamaterial Using MEMS Mechanism," IEEE J. Sel. Top. Quantum Electron. **21**, 2700207 (2015).
26. J. Liu and Z. Hong, "Mechanically tunable dual frequency THz metamaterial filter," Opt. Commun. **426**, 598–601 (2018).
27. K. M. Devi, D. R. Chowdhury, G. Kumar, and A. K. Sarma, "Dual-band electromagnetically induced transparency effect in a concentrically coupled asymmetric terahertz metamaterial," J. Appl. Phys. **124**(6), 063106 (2018).
28. K. M. Devi, M. Islam, D. R. Chowdhury, A. K. Sarma, and G. Kumar, "Plasmon-induced transparency in graphene-based terahertz metamaterials," EPL **120**(2), 27005 (2017).
29. K. M. Devi, A. K. Sarma, D. R. Chowdhury, and G. Kumar, "Plasmon induced transparency effect through alternately coupled resonators in terahertz metamaterial," Opt. Express **25**(9), 10484–10493 (2017).
30. J. Wang, B. Yuan, C. Fan, J. He, P. Ding, Q. Xue, and E. Liang, "A novel planar metamaterial design for electromagnetically induced transparency and slow light," Opt. Express **21**(21), 25159–25166 (2013).
31. C. Shu, Q. Chen, J. Mei, and J. Yin, "Analogue of tunable electromagnetically induced transparency in terahertz metal-graphene metamaterial," Mater. Res. Express **6**(5), 055808 (2019).
32. X. R. Jin, J. Park, H. Y. Zheng, S. Lee, Y. Lee, J. Y. Rhee, K. W. Kim, H. S. Cheong, and W. H. Jang, "Highly dispersive transparency at optical frequencies in planar metamaterials based on two-bright-mode coupling," Opt. Express **19**(22), 21652–21657 (2011).
33. J. S. Hwang, Y. J. Kim, Y. J. Yoo, K. W. Kim, J. Y. Rhee, L. Y. Chen, S. R. Li, X. W. Guo, and Y. P. Lee, "Tunable quad-band transmission response, based on single-layer metamaterials," Opt. Express **26**(24), 31607–31616 (2018).
34. N. Born, M. Scheller, M. Koch, and J. V. Moloney, "Cavity enhanced terahertz modulation," Appl. Phys. Lett. **104**(10), 103508 (2014).
35. X. Li, T. Yang, W. Zhu, and X. Li, "Continuously tunable terahertz metamaterial employing a thermal actuator," Microsyst. Technol. **19**(8), 1145–1151 (2013).
36. D. R. Chowdhury, N. Xu, W. Zhang, and R. Singh, "Resonance tuning due to Coulomb interaction in strong near-field coupled metamaterials," J. Appl. Phys. **118**(2), 023104 (2015).
37. C. M. Soukoulis, M. Kafesaki, and E. N. Economou, "Negative-Index Materials: New Frontiers in Optics," Adv. Mater. **18**(15), 1941–1952 (2006).
38. W. Y. Chang and Y. S. Hsihe, "Multilayer microheater based on glass substrate using MEMS technology," Microelectron. Eng. **149**, 25–30 (2016).
39. C. Z. Tan, "Review and analysis of refractive index temperature dependence in amorphous SiO2," J. Non-Cryst. Solids **238**(1-2), 30–36 (1998).